Numerical study of failure modes of hazardous material tanks exposed to fire accidents in the process industry

Mo, Li; Xiao, Shenbin; Chen, Hang; Tan, Xinxin; Yang, Ming; Reniers, Genserik; Chen, Chao

DOI
10.1002/prs.12643

Publication date
2024

Document Version
Final published version

Published in
Process Safety Progress

Citation (APA)
Mo, L., Xiao, S., Chen, H., Tan, X., Yang, M., Reniers, G., & Chen, C. (2024). Numerical study of failure modes of hazardous material tanks exposed to fire accidents in the process industry. *Process Safety Progress*, *43*(4), 760-773. https://doi.org/10.1002/prs.12643

Important note
To cite this publication, please use the final published version (if applicable).
Please check the document version above.

Received: 13 May 2024 | Revised: 11 July 2024 | Accepted: 30 July 2024

DOI: 10.1002/prs.12643

PROCESS SAFETY PROGRESS

ORIGINAL ARTICLE

Numerical study of failure modes of hazardous material tanks exposed to fire accidents in the process industry

Li Mo[1] | Shenbin Xiao[1] | Hang Chen[2] | Xinxin Tan[3] | Ming Yang[4] | Genserik Reniers[4,5,6] | Chao Chen[3,7]

[1]School of Mechanical and Electrical Engineering, Southwest Petroleum University, Chengdu, China

[2]AVIC Chengdu CAIC Electronics Co. Ltd., Chengdu, China

[3]Petroleum Engineering School, Southwest Petroleum University, Chengdu, China

[4]Safety and Security Science Group, Faculty of Technology, Policy and Management, TU Delft, Delft, The Netherlands

[5]Faculty of Applied Economics, Antwerp Research Group on Safety and Security (ARGoSS), University Antwerp, Antwerp, Belgium

[6]CEDON, KULeuven, Campus Brussels, Brussels, Belgium

[7]China Academy of Safety Science and Technology, Beijing, China

Correspondence
Chao Chen, Petroleum Engineering School, Southwest Petroleum University, Chengdu 610500, China.
Email: chenchaoswpu@gmail.com

Funding information
Sichuan Province Science and Technology Support Program, Grant/Award Number: 2023YFS0412

Abstract

Fire accidents in oil tank farms can trigger domino effects, leading to multiple tank fires with catastrophic consequences. Preventing losses in large-scale tank farms requires a dynamic assessment of fire-induced domino accidents. Existing research often focuses on calculating the time to failure (TTF) of storage tanks but overlooks the influence of failure modes. This study develops numerical models to explore failure modes of oil storage tanks with uniform and stepwise walls exposed to thermal radiation. Factors such as the flame heights of combustion tank, adjacent spacings, wall thickness, and tank volumes are considered. The numerical model employs a solid double-layer flame model to determine thermal radiation intensity and temperature, followed by a dynamic stress–strain and buckling analysis to obtain time to buckling (TTB) and time to yielding (TTY). If TTB < TTY, the failure model is buckling; otherwise, the failure model is yielding. Results indicate that failure modes in nonuniform thermal fields include buckling and yielding, with stepwise walls favoring buckling and uniform walls favoring yielding. When the wall thickness is below the critical value, failure is yielding; otherwise, it is buckling. These findings support risk management and emergency response for fire-induced domino effects in oil tank farms.

KEYWORDS
domino effect, failure modes, pool fire, storage tank, time to failure

1 | INTRODUCTION

Petroleum products such as gasoline, diesel, and kerosene are typically flammable and explosive chemicals and are always stored in oil tank farms with multiple storage tanks.[1] Storage tanks hold a high position in the socical economy.[2] Consequently, there is a significant risk of fire or explosion in a tank farm, possibly triggering a second or even more severe accident in an adjacent tank and resulting in domino effects.[3] Pool fires frequently occur in domino effect accidents since thermal radiation induced by the fire can weaken the strength and damage the structure of nearby storage tanks.[4–7] Besides, multiple fires may occur in oil storage tanks and lead to synergistic effects, increasing the risk of domino effects.[8–10] For instance, on March 17, 2019, a fire occurred at an oil tank farm of the Intercontinental Terminals Company (ITC) in Houston, USA, triggering domino effects and damaging multiple tanks.[11]

To prevent domino effects from the fire, it is essential to explore the failure mechanism of storage tanks under the thermal radiation. In fire scenarios, intense heat loads gradually weaken the shell material of adjacent tanks, leading to damage in the target tanks.[12] The damage may be divided into two types: buckling failure and yield failure.[13,14] Buckling failure refers to the sudden and rapid change in shape (deformation) of storage tanks under nonuniform heat loads, while yield failure is caused by the reduction of yield strength due to the increased temperature of the tank material.[14,15] The time elapsed between the onset of heating on the target tank and its eventual failure is referred

to as the "time to failure" (TTF).[16] As a result, to prevent and mitigate the domino effect of the fires, it is essential to explore the failure modes and TTF of storage tanks in fire scenarios.

Rebec et al. performed a blend of numerical and experimental analyses to scrutinize the radiation characteristics of the burning tank, assess the distribution of radiation in adjacent tanks, and explore the impact of the fuel level within the tank.[17] Wang et al. conducted a numerical investigation to analyze both the individual and collective impacts of the combustion tank on their thermophysical characteristics and the distribution of radiation flux.[18] Batista-Abreu et al. demonstrated the crucial role of thermal gradients within the tank thickness concerning both buckling and mode.[19] Landucci et al. employed a structural model to appraise the domino effect triggered by fires and indicated a direct correlation between the failure time of pressure vessels and the heat radiation intensity from the fire.[20] Liu first conducted a comprehensive and systematic research on the thermal properties and structural alterations of storage tanks in the vicinity of a fire and showed that the different temperature distributions of the tanks and the thin-walled shell structure are the key elements for the occurrence of the buckling failure under thermal radiation.[21] Godoy et al. extended Liu's simplified temperature field expression to study the equilibrium state of fixed-roof tanks with uniform wall thicknesses and showed that in tanks without stored media, thermal expansion occurs before thermal buckling and that the deformation of the lower tank region transitions from outward thermal expansion to inward depression.[22] Cozzani et al. highlighted the interconnection between predicting fire and domino effects in tanks and the thermodynamic properties of pressure vessels and emphasized that the prediction of these effects depends on considering both the pressure within the tanks and the thermodynamic properties of pressure vessels.[23] Pantousa employed a solid flame model to investigate the thermal buckling of storage tanks with uniform wall thicknesses under different pool fire scenarios.[24] Li et al. highlighted that the thermal buckling mode observed in vaulted tanks with stepped wall thicknesses falls under elastic buckling and the nonlinear nature of the thermal buckling behavior.[25] Dong et al. investigated thin-walled structures, which are more prone to buckling when subjected to axial pressure or shear loads, in the context of optimizing plate and shell structures.[26] Pantousa and Godoy conducted a numerical investigation of the stress distribution in storage tanks using three different linear methods.[27] Pourkeramat et al. numerically investigated the impact of wind load and flame smoke on the stability of the tank structure exposed to adjacent fires.[28]

Although many studies have explored the failure of storage tanks exposed to fire scenarios, it is still difficult to identify the failure modes of different tanks in different fire scenarios. This study makes an important scientific contribution to the determination of failure modes of the storage tanks. Besides, the failure model may have a significant influence on the TTF; thus, neglecting the failure mode may lead to an inaccurate TTF, resulting in unreasonable prevention and mitigation strategies and accelerating the propagation of fire.

Therefore, in this study, a numerical model of the thermal response of the storage tanks is established to explore the failure modes in different scenarios, considering the influence of the flame heights of combustion tank, adjacent spacings, wall thickness, and tank volumes. Section 2 establishes the numerical model of storage tanks exposed to fire, and the results are presented in Section 3. Section 4 discusses the influence of key parameters on the failure modes and failure time. The conclusions derived from this study are elaborated in Section 5.

2 | ESTABLISHMENT OF THE NUMERICAL MODEL

This paper utilizes the finite element analysis software ABAQUS to analyze the sequential thermodynamic coupling of the storage tanks. The establishment of the failure numerical model of storage tanks exposed to fire includes geometric modeling, flame modeling, buckling modeling, and yielding modeling.

2.1 | Geometric modeling

Steel storage tanks are widely used in the petrochemical industry for storing petroleum products and other materials.[29] The material of the tank is Q345 steel, and the inner and outer surfaces have distinct emissivity values. Additionally, it is important to note that the thermal-physical properties of the Q345 vary as a function of temperature. The density of Q345 material is 7850 kg/m^3, which remains constant with increasing temperature.[30] The average convective heat transfer coefficient between the storage tank and air is denoted as $\overline{h_c}$ (W/m^2 K).[17] This coefficient can be calculated using Equation (1):

$$\overline{h_c} = N_u K_a / L^* \tag{1}$$

where N_u is the Nussle number, K_a is the thermal conductivity of air (W/[m K]), and L^* is the height of storage tank (m). The Nusselt number in the laminar flow regime is denoted as N_u, and its calculation formula is

$$N_u = 0.664 R_e^{\frac{1}{2}} P_r^{\frac{1}{3}} \tag{2}$$

where P_r is the Prandtl number (which takes a value of about 0.703 for air), and R_e is the Reynolds number. Reynolds number R_e is calculated as

$$R_e = u_\infty L^* / \upsilon \tag{3}$$

where υ is the dynamic viscosity of air (m^2/s). When $R_e < 10^5$ for laminar flow, it implies that all wind speeds except the free-field wind speed are considered turbulent. In the scenario where $u_\infty = 0$ (no-wind condition), indicating laminar flow, we consider a small wind scenario with $u_\infty = 0.1$ m/s, and substitute this value into the calculation.

In this paper, a vertical vaulted empty storage tank is considered; when it undergoes combustion, it becomes a source of fire for nearby

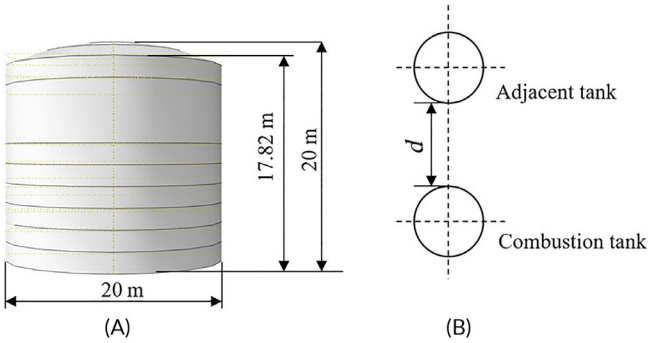

FIGURE 1 Simplified model of oil storage tanks. (A) Simplified model of adjacent tank. (B) Top view of storage tank.

TABLE 1 Structural parameters of the storage tank.[32]

Name	Material	Height (m)	Thickness (mm)
1st shell course	Q345	1.78	13
2nd shell course	Q345	1.78	12
3rd shell course	Q345	1.78	11
4th shell course	Q345	1.78	10
5th shell course	Q345	1.78	9
6th shell course	Q345	1.78	7
7th–9th shell course	Q345	1.78	6
10th shell course	Q345	1.80	6

storage tanks, referred to as a combustion tank. The storage tank exposed to thermal radiation from the combustion tank is termed the adjacent tank. Figure 1 indicates that both the adjacent tank and the combustion tank have identical diameter (D) and height (H). The design of the target tank adheres to the engineering requirements for vertical vaulted storage tanks.[31] The configuration consists of 10 layers of tanks, each with a height of 1.78 m, resulting in a total volume of 5000 m^3. The structural parameters of the storage tank are listed in Table 1.[32]

2.2 | Flame model

The thermal radiation emitted by the flame is contingent upon the chosen flame model, and the solid flame model is a widely employed semi-empirical model.[33] Semi-empirical radiation models include the point source radiation model, the solid flame model, and the line source radiation model.[34] The solid flame model shows enhanced efficacy in foreseeing radiative heat flux from targets situated under the flame boundaries.[35–37] This paper thus employs a cylindrical solid flame model with petroleum as the fuel source, categorizing the flame into two regions. Under windless conditions, the solid double flame model collectively assumes the form of a vertical cylinder. The characteristic

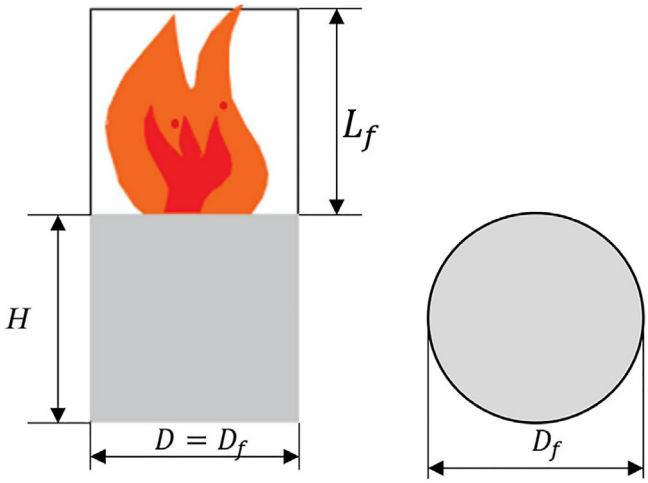

FIGURE 2 Parameters of the flame model.

parameters of the flame model in the windless scene are shown in Figure 2. The key parameters characterizing the flame's geometry include the cross-sectional shape, flame diameter (D_f), and flame length (L_f). In windless conditions, the flame diameter matches the diameter of the combustion canister, and the cross-sectional shape is circular.

In a windless scenario, the flame length L_f can be calculated using the expression[38]

$$L_f = 42D_f \times (m^*)^{0.61} \tag{4}$$

where D_f is the bottom diameter of the combustion tank (m); m^* is the dimensionless mass burning rate (which is described in detail in the reference manual).[39] The length of the bright portion of flame can be obtained from Equation (5)[40]:

$$L_1 = 11.404\,(m^*)^{1.13}(u^*)^{0.179}\left(\frac{N_c}{N_H}\right)^{-2.49} D_f \tag{5}$$

where L_1 is the length of the bright portion of flame (m); N_C, N_H represent the quantities of chemical atoms within the material parameters of the flame model; and u^* is dimensionless wind speed. The total height of the flame is denoted by the variable L_f, and u^* is dimensionless wind speed.[41] To account for the influence of smoke, the average emissive power ($E_{av\text{-}max}$) of the flame model is calculated using Equation (8) in the solid double flame model:

$$m^* = m_b / \left[\rho (gD_f)^{0.5}\right] \tag{6}$$

$$m_b = m_{max}\left(1 - e^{-k_\beta D_f}\right) \tag{7}$$

where m_b is mass rate of burning (kg/m^2 s); ρ is air density (kg/m^3); g is acceleration of gravity; D_f is diameter of the tank (m); m_{max} is s the

maximum burning rate (kg/m^2 s); and k_β is an empirical coefficient of fuel.[24]

$$E_{av-max} = E_{max}\,\mathrm{Exp}(-0.12D_f) + E_{soot}[1 - \mathrm{Exp}(-0.12D_f)] \quad (8)$$

The emission power of the bright flame is denoted as $E_{max} = 140$ kW/m^2, while the emission power of the dark flame is represented as $E_{soot} = 20$ kW/m^2. Equation (9) providess a numerical computation method to calculate the temperature of the flame model in both light and dark flame conditions[42]:

$$T_{fe} = \sqrt[4]{\frac{\varepsilon\sigma T_a^4 + E_{av}\tau}{\varepsilon\sigma}} \quad (9)$$

where T_{fe} is the equivalent temperature of the flame surface (°C); and E_{av} is for the surface temperature of each region of the flame model. Each region's temperature is determined by substituting the emissive power, and ε is the flame emissivity, which takes the value of 1, σ is the Stefan-Boltzmann constant, which takes the value of 5.67×10^{-8} W/m^2/K^4. τ is atmospheric transmittance, which depends on the distance d between the adjacent tank and the combustion tank.[42]

In the solid flame model, the flame is represented as a cylinder. Equations (10) and (11) give the horizontal and vertical view factors of the tank relative to the two flame areas[33]:

$$F_H = \frac{1}{\pi}\left[\frac{(B-1/S)}{\sqrt{B^2-1}}\tan^{-1}\sqrt{\frac{(B+1)(S-1)}{(B-1)(S+1)}} - \frac{(A-1/S)}{\sqrt{A^2-1}}\tan^{-1}\sqrt{\frac{(A+1)(S-1)}{(A-1)(S+1)}}\right] \quad (10)$$

$$F_V = \frac{1}{\pi}\left[\frac{1}{S}\tan^{-1}\frac{h}{\sqrt{S^2-1}} + \frac{h}{s}\left\{\tan^{-1}\sqrt{\frac{S-1}{S+1}} - \frac{A}{\sqrt{A^2-1}}\tan^{-1}\sqrt{\frac{(A+1)(S-1)}{(A-1)(S+1)}}\right\}\right] \quad (11)$$

where h is flame height or radius (m), S is distance to the observer from axis (m), $A = \frac{h^2+S^2+1}{2S}$, and

$$B = \frac{S^2+1}{2S}.$$

2.3 | Buckling modeling

The ADM algorithm (artificial damping method) is widely adopted for solving thermal buckling problems and has been utilized by numerous researchers.[21,24,27] This method iterates adaptively during the solution process and effectively detects and manages local buckling phenomena, contributing to algorithm convergence. Its effectiveness in solving thermal buckling and detecting local buckling has been verified by phenomena through algorithmic and experimental comparisons.[21] This study adopts the ADM formulation for thermal buckling analysis of storage tanks:

$$P - Q - F_D = 0 \quad (12)$$

$$F_D = c \times M^* \times v \quad (13)$$

$$v = \frac{\Delta u}{\Delta t} \quad (14)$$

where M^* is the artificial mass matrix per unit density, v is the velocity vector of the node (m/s), Δu is node displacement (m), Δt is the time increment (s), and c is the damping ratio. A rapid change in the damping ratio signifies local instability and indicates thermal buckling of the storage tank.

2.4 | Yield modeling

The yield strength of a storage tank is the maximum stress that the tank material can withstand before experiencing plastic deformation. When subjected to thermal radiation within the burning tank, the tank temperature rises gradually, and thermal stress is generated within the tank structure due to differential expansion and contraction of its materials. Tank failure occurs when the thermal stress of the tank surpasses its ultimate strength threshold. In this study, the calculation method of yield strength of steel provided by European Convention on Construction of Steel (ECCS) is selected for yielding analysis, as follows[32]:

$$\frac{\sigma_s^T}{\sigma_s^{20}} = 1 + \frac{T}{767\ln\left(\frac{T}{1750}\right)}\ 0 \le T \le 600^\circ\mathrm{C} \quad (15)$$

$$\frac{\sigma_s^T}{\sigma_s^{20}} = 108\frac{1 - \frac{T}{1000}}{T - 400}\ T > 600^\circ\mathrm{C} \quad (16)$$

where σ_s^T is the yield strength of storage tank at different temperatures T (MPa); σ_s^{20} is the yield strength of the storage tank at 20°C (MPa); and T represents the temperature of the tank at various intervals during combustion (°C).

2.5 | Numerical model verification

This study reproduces Liu's numerical study to verify the numerical model. The adjacent tank is assumed to be empty, and the tank dimensions are as set by Liu.[21] The thermal buckling of the storage tank across various temperature fields is depicted in Figure 3. Figure 3A shows the results obtained by Liu's thermal buckling, and Figure 3B shows the results obtained by the developed numerical model. The structural deformation of the storage tank is manifested in the lower region of tank on the highest temperature side for both figures, and the deformation patterns are also identical. Figure 4 illustrates the meridional and peripheral stresses along the height of the adjacent tank at the most heated meridian. The stress appears at the upper and bottom regions of the cylindrical tank

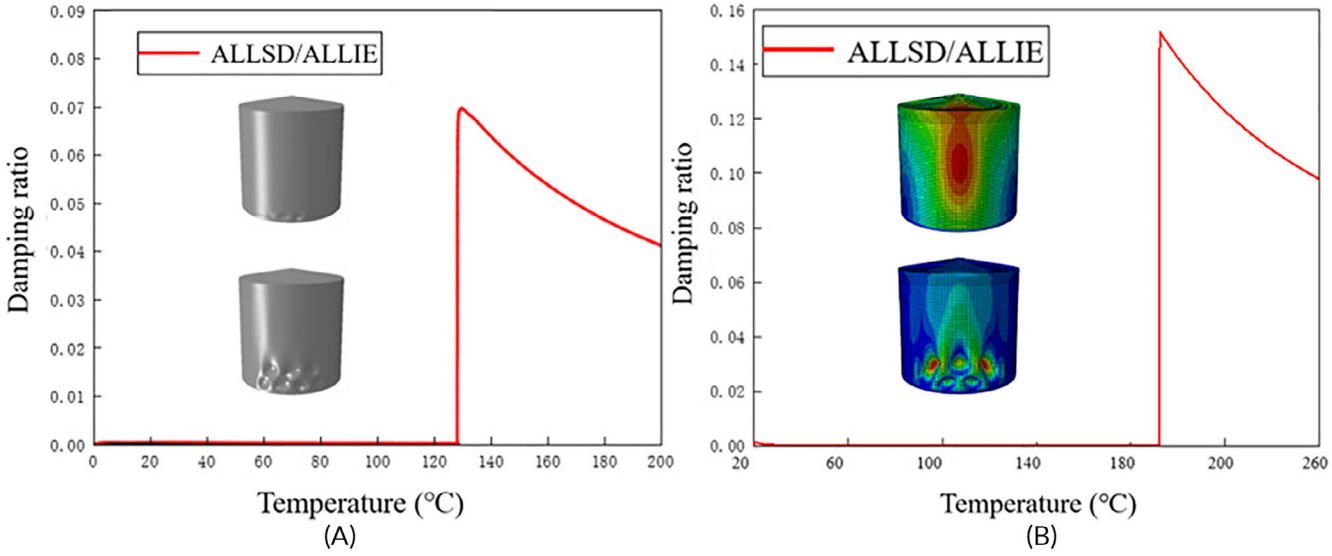

FIGURE 3 Comparison of results between Liu's numerical model and the developed numerical model. (A) Damping radio in Liu's numerical model. (B) Damping radio in the developed numerical model.

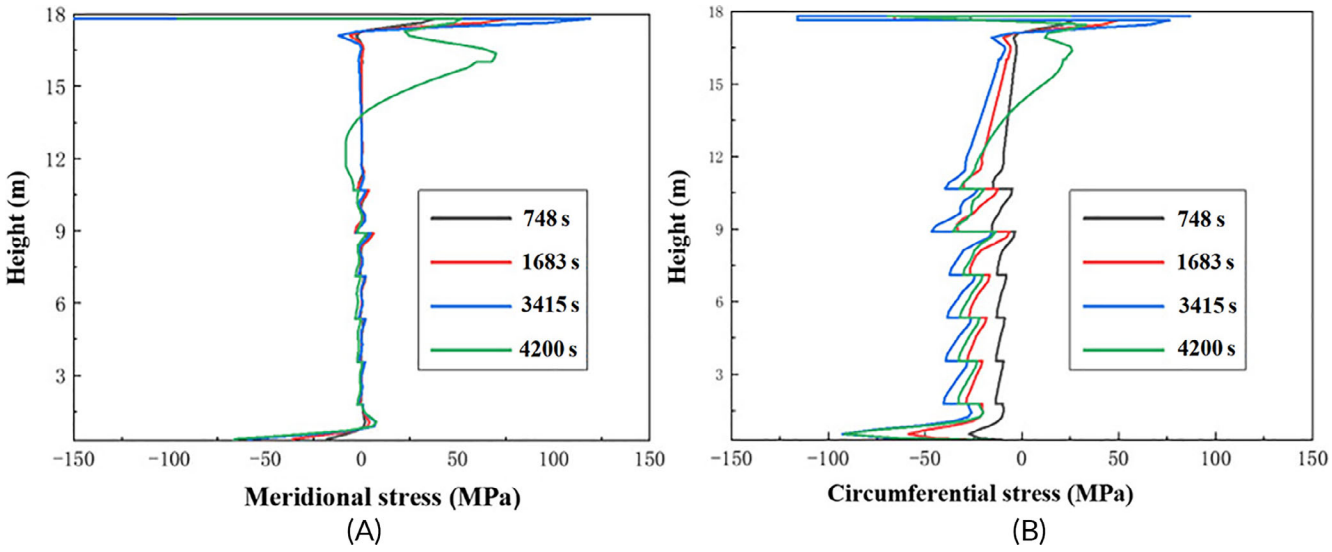

FIGURE 4 Meridional stresses and circumferential stresses along the height of the tank ($\theta = 0^{\circ}$). (A) Meridional stresses of the adjacent tank. (B) Circumferential stresses of the adjacent tank.

wall, and the distributions of stresses are consistent with Li's numerical model.[25] It can be concluded that the numerical model developed in this study is an effective tool for predicting and analyzing the failure of storage tanks.

3 | MODEL RESULTS

The numerical model developed in Section 2 is implemented by the widely used nonlinear analysis software Abaqus. The model is constructed using shell units (DS4), and the mesh consists of hexahedral elements oriented in the circumferential and vertical directions. In this study, the mesh of the cylinder-to-roof joint adopts the refined element because temperature changes rapidly in this zone due to a sudden change of the view factor. The total number of meshes is 23,530. The adjacent tank thermal boundary conditions include radiation from the flame, convection to surrounding air, and heat conduction of all tank walls. The combustion tank's thermal boundary condition is radiation to the external surface of adjacent tank. The numerical analysis includes temperature field analysis, thermal buckling analysis, and thermal yielding analysis.

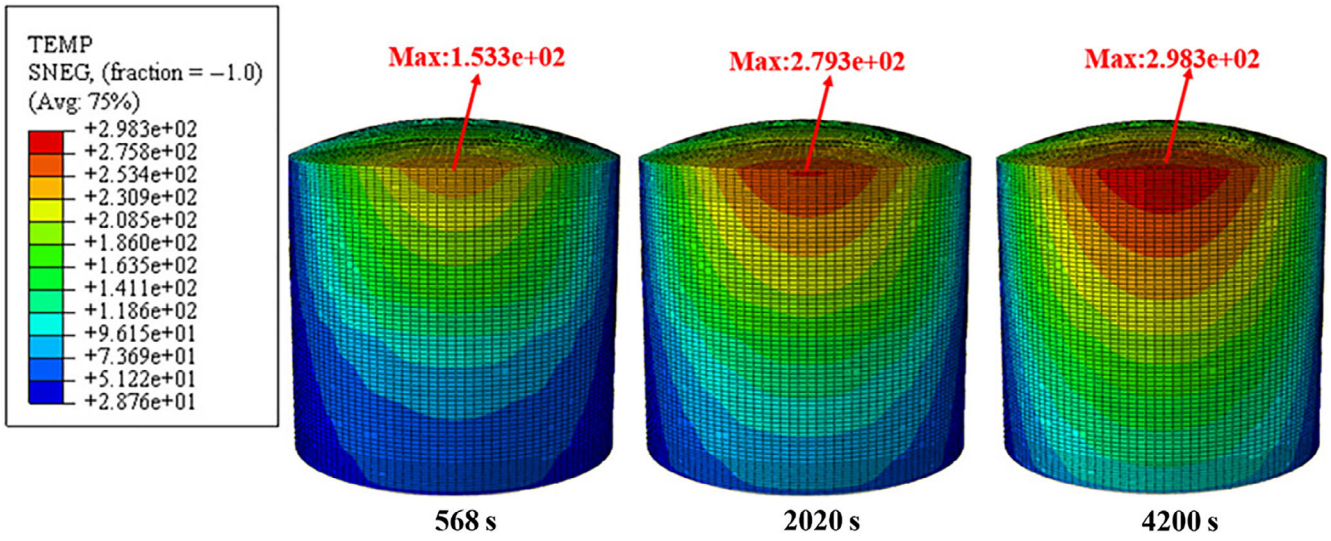

FIGURE 5 Temperature distribution of the storage tank during the warming process.

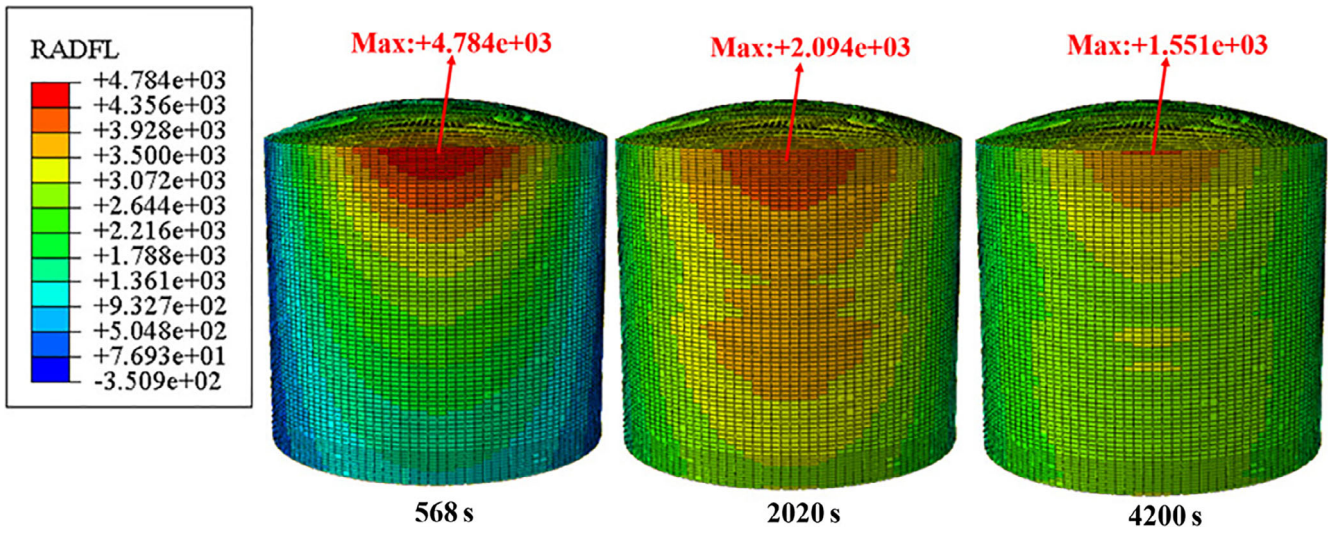

FIGURE 6 Radiant heat flux distribution of the storage tank during the warming process.

3.1 | Temperature field analysis

Figures 5 and 6 display the temperature field and radiant heat flux changes of the adjacent tank, respectively. The temperature distribution is symmetric along the central axis, with the highest temperatures and radiant heat flux primarily at the junction between the tank roof and upper portion of tank wall. The radiant heat flux of the adjacent tank steadily decreases over time, leading to an increase in its temperature until it reaches its maximum value (298.3°C). However, differences in the viewing angle factor for each region relative to the flame increase the temperature and radiant heat flux distribution disparities of the different regions.

3.2 | Thermal buckling analysis of storage tanks

Figure 7 illustrates the displacement of maximum deformation point and the damping ratio c changing with time of the adjacent tank under thermal rediation. Figure 7A shows that the tank's displacement is positive until reaching point A, at which the damping ratio c approaches zero. After point A, the tank exhibits fold deformation, and the damping ratio c rapidly increases and then decreases. The radial displacement becomes negative, indicating a transition from outward thermal expansion to inward concavity. The axial displacement reduces to a certain extent, but overall it is still positive, which is because of the constraint of the tank top and the small difference in axial temperature difference. Figure 7B shows that the damping ratio

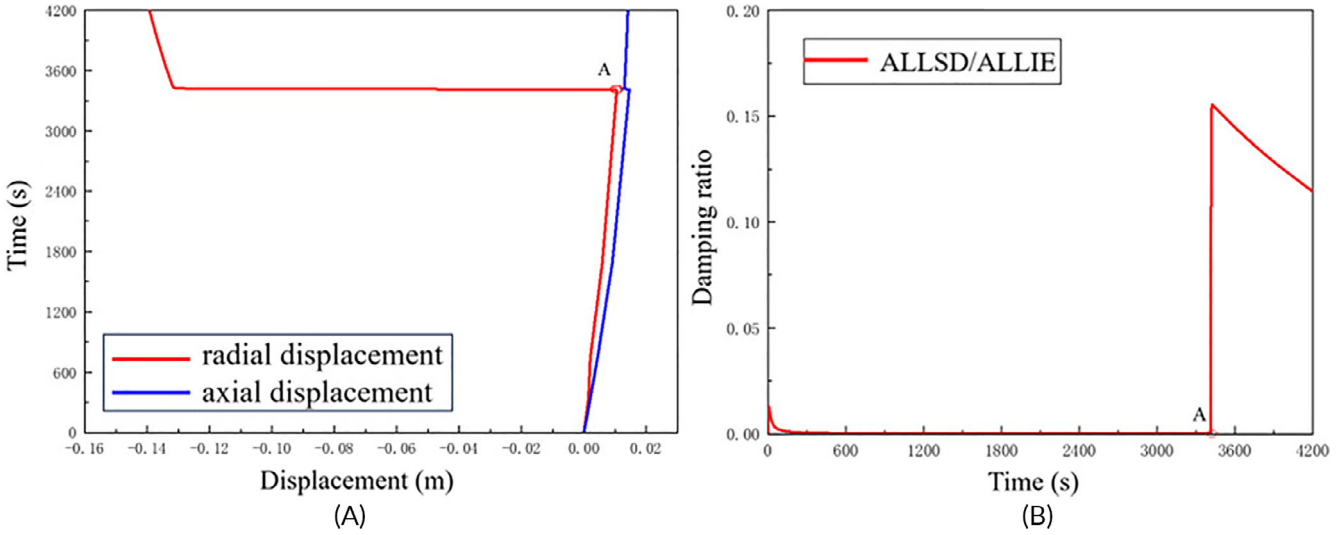

FIGURE 7 Variation of displacement and damping ratio of the storage tank. (A) Variation process of displacement. (B) Variation process of damping ratio with time.

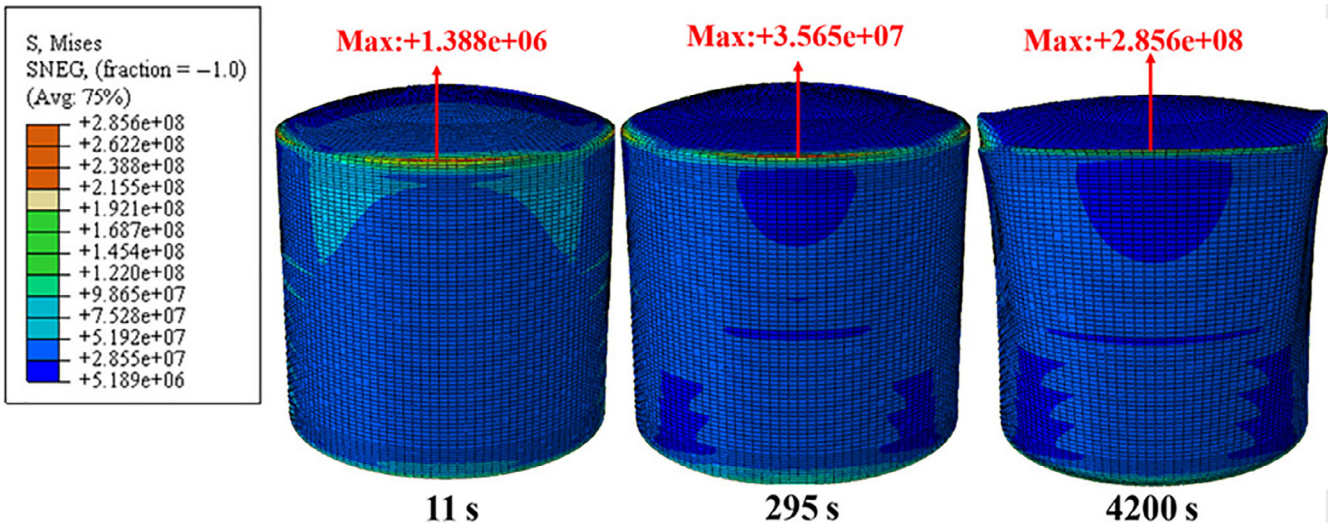

FIGURE 8 Stress distribution of storage tank.

rapidly increases, leading to a sudden change in the tank's geometry, resulting in nonlinear deformation and degradation of structural stability. Thus, point A is defined as the time to buckling (TTB) and the temperature of storage tank at this time is the buckling temperature (T_0), which is employed as one of the criteria for distinguishing the failure mode of the storage tank.

3.3 | Thermal yield analysis of storage tanks

Temperature variation of the storage tank causes different parts of tank to constrain each other, limiting their ability to expand and contract freely. Consequently, the storage tank experiences varying degrees of thermal stress and thermal strain. Nonuniform distribution in the temperature field of the adjacent tank is attributed to variations in the angle factors between the adjacent tank and the combustion tank. Figures 8 and 9 show the stress and strain of the storage tank as the persistence of thermal radiation to the tank. The maximum stress and strain of the storage tank are primarily concentrated at the junction of the upper section and the top of the tank. The bottom of the tank shows minimum deformation, while the top of the tank shows the most pronounced deformation. The stress of the storage tank gradually increases while the strain decreases. This is because the distribution of the temperature field directly determines the stress and strain distribution of the storage tank. The varying temperature distribution induces thermal expansion and contraction, resulting in localized stresses and strains of the tank structure.

4 | DISCUSSION

Based on the simulation results in Section 3, this section discusses critical factors that have an important impact on the failure modes of storage tanks exposed to fire, to support the determination of failure modes of storage tanks in diverse scenarios.

4.1 | Effets of uniform tanks and stepwise tanks

This section investigates the failure modes of stepwise and uniform tanks. Figure 10 shows the deformation process of the maximum displacement point of the stepwise tank and the uniform tank in thermal buckling. At the critical time point of TTB, the deformation and

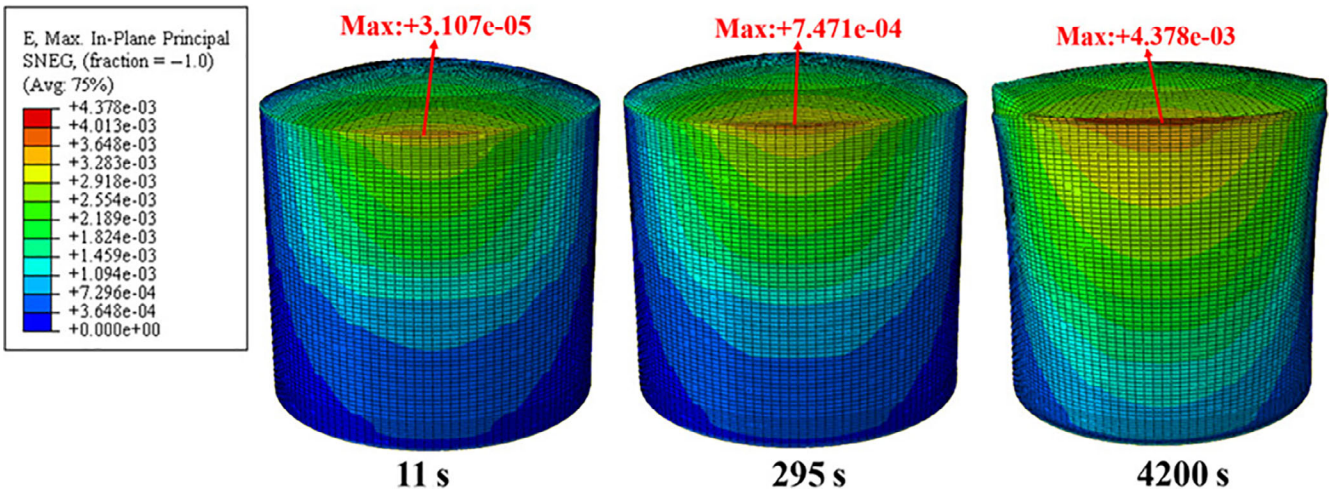

FIGURE 9 Strain distribution of the storage tank.

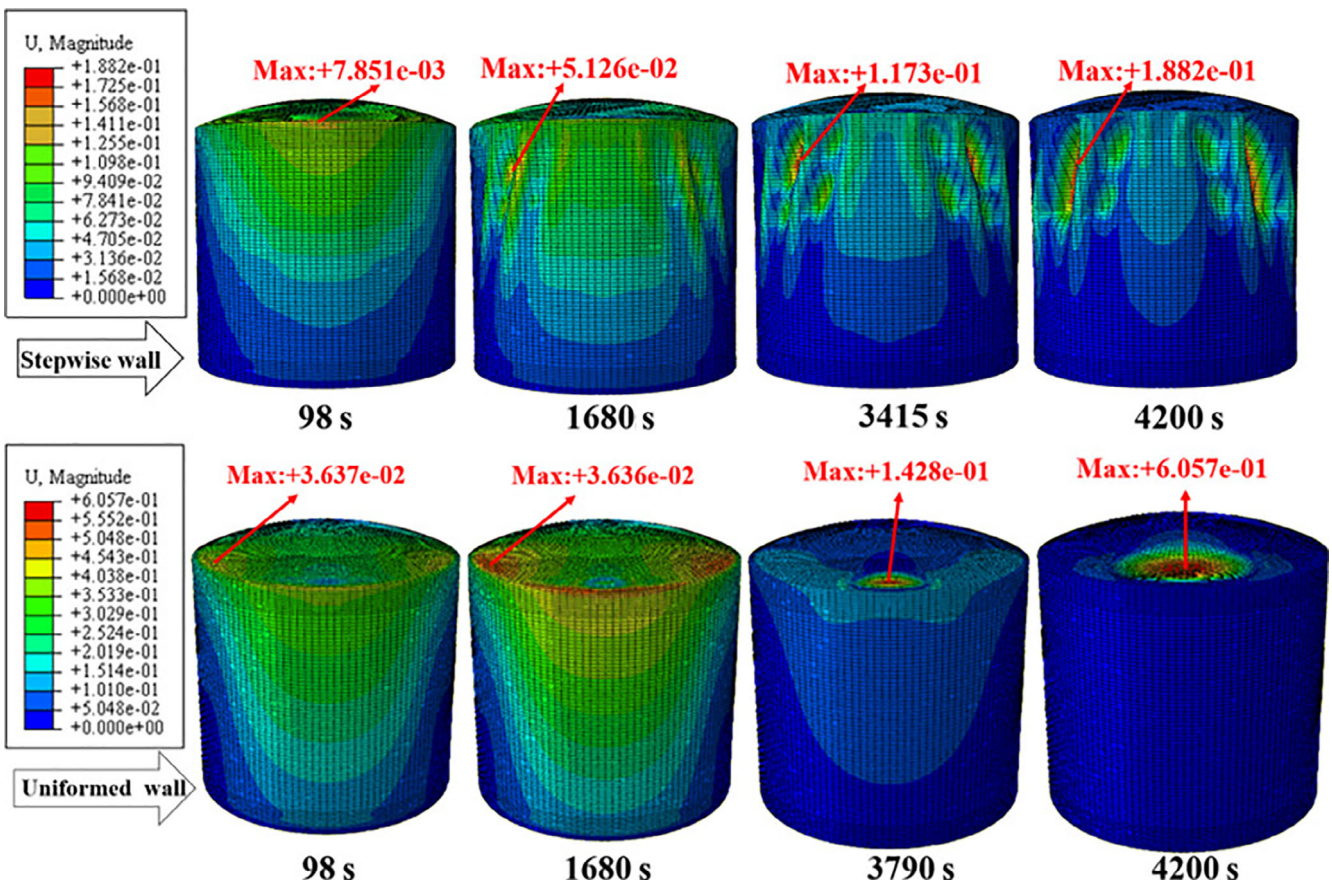

FIGURE 10 Deformation process of the storage tank with stepwise wall and uniform wall.

depression areas of the stepwise tank primarily occur in the upper regions, whereas those of the uniform tank manifest in the roof areas. This is because the wall thickness of the uniform tank is 13 mm, and the thickness of the roof is 5 mm. Compared with the stepwise tank, the structural differences are more obvious, resulting in the stress of the storage tank mainly appearing on the tank roof, which is concentrated and shrinks inward.

Figure 11 provides a comparative analysis of the TTY between the stepwise tank and uniform tank. The failure mode of the stepwise tank is yielding, while the failure mode of the uniform tank is buckling. This is because the bending and tensile strength of stepwise tank are reduced, the stability and load-bearing capacity of the tank structure are reduced, and the tank is more prone to large nonlinear deformation and strength failure. Besides, the wall thickness of the uniform storage tank increases, and the thick material has a stacking effect, which makes the uniform tank to have better resistance to geometric shape mutations. Thus the yield strength of the uniform tank increases, leading to the tank to preferentially buckle. The results can be applied to assess failure modes resulting from uniform tanks and stepwise tanks in fire scenarios.

4.2 | Effect of the flame heights of combustion tank

The thermal radiation received by adjacent tanks depends on the flame heights of the combustion tank. Therefore, the impact of

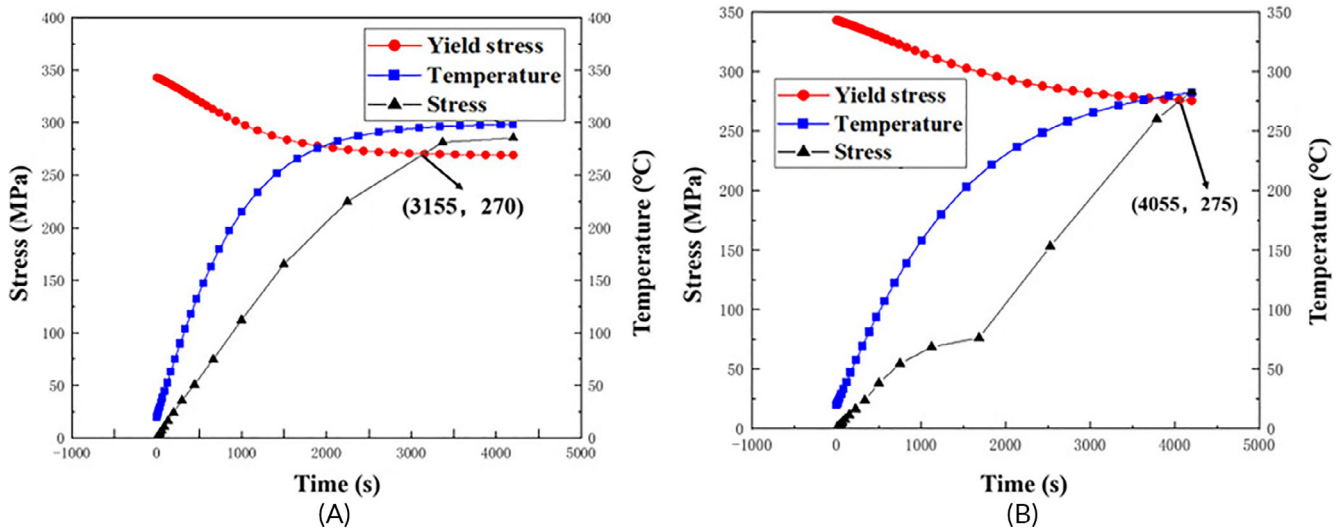

FIGURE 11 Comparison of time to yielding (TTY) between the stepwise tank and uniform tank. (A) TTY of stepwise storage tank. (B) TTY of uniformed storage tank.

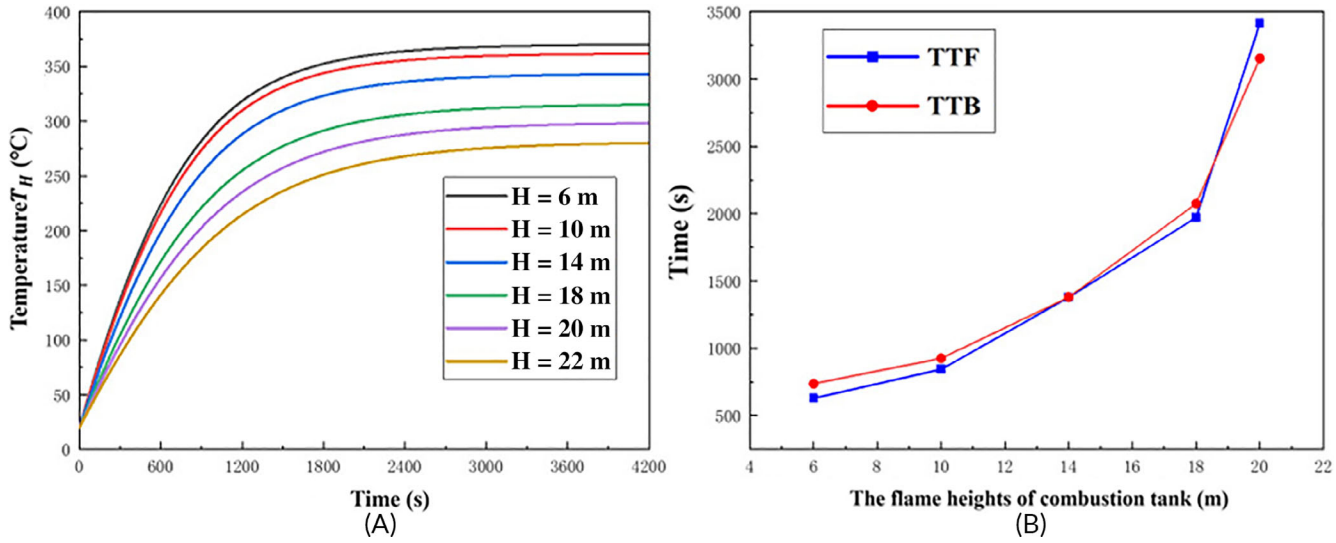

FIGURE 12 Parameters in thermal post-buckling and post-yielding under different the flame heights of the combustion tank. (A) Comparison of T_H. (B) Comparison of time to buckling and time to yielding.

the flame heights of the combustion tank on the failure mode and TTF of the adjacent tank is investigated. Figure 12A illustrates the variation in the maximum temperature (T_H) of the adjacent tank at different flame locations. The maximum temperature of the adjacent tank tends to stabilize at around 4200 s. The maximum temperature (T_H) decreases with increasing the flame heights of the combustion tank. This is because the heating rate of the adjacent tank slows down with increasing maximum temperature (T_H) and decreases with increasing the flame heights of the combustion tank. Figure 12B presents a comparison of TTB and TTY at various the flame heights of the combustion tank. Additionally, Table 2 summarizes the relevant parameters of adjacent tanks for each the flame height of combustion tank (H). When the flame height of the combustion tank is less than 20 m, there is a positive correlation between the critical yield temperature of the tank and the flame height of combustion tank. As the flame height of the combustion tank increases, the critical yield temperature of the storage tank decreases.

It can be observed that the TTB and TTY of the storage tank are prolonged as the flame heights of combustion tank increases. When the flame height of combustion tank is less than 20 m, the storage tank primarily experiences post-thermal buckling. For a flame height of the combustion tank of 20 m, the storage tank first undergoes yielding and then buckling. However, when the flame height of the combustion tank is 22 m, the storage tank does not experience post-thermal buckling. This is because of the different viewing angle factors between the adjacent tank and the combustion tank. The total height of the tank is 20 m, and when the flame height of the combustion tank is the same, thermal deformation of the storage tank is reduced, resulting in temperature distribution to change slightly in the storage tank. This reduction in temperature changes decreases the possibility of thermal buckling, thus causing the preferential occurrence of thermal yielding. The results can be applied to evaluate the failure modes of storage tanks under various levels of fire scenarios.

TABLE 2 Parameters corresponding to different the flame heights of combustion tank.

H (m)	TTB (s)	T_0 (°C)	TTY (s)	T_S (°C)
6	630	230.574	737	284.314
10	844	264.752	926	269.465
14	1378	299.324	1380	268.066
18	1972	300.073	2075	255.599
20	3415	270.373	3155	276.024

Abbreviations: TTB, time to buckling; TTY, time to yielding.

4.3 | Effect of adjacent spacings

Adjacent spacing is defined as the distance between the adjacent tank and the combustion tank. The variation of the maximum temperature (T_H) of the adjacent tank under different adjacent spacings is

TABLE 3 Parameters corresponding to different adjacent spacings.

d (m)	TTB (s)	T_0 (°C)	TTY (s)	T_S (°C)
15	3026	324.272	3332	257.993
20	3415	270.373	3155	276.024
25	2787	263.580	3330	280.784

Abbreviations: TTB, time to buckling; TTY, time to yielding.

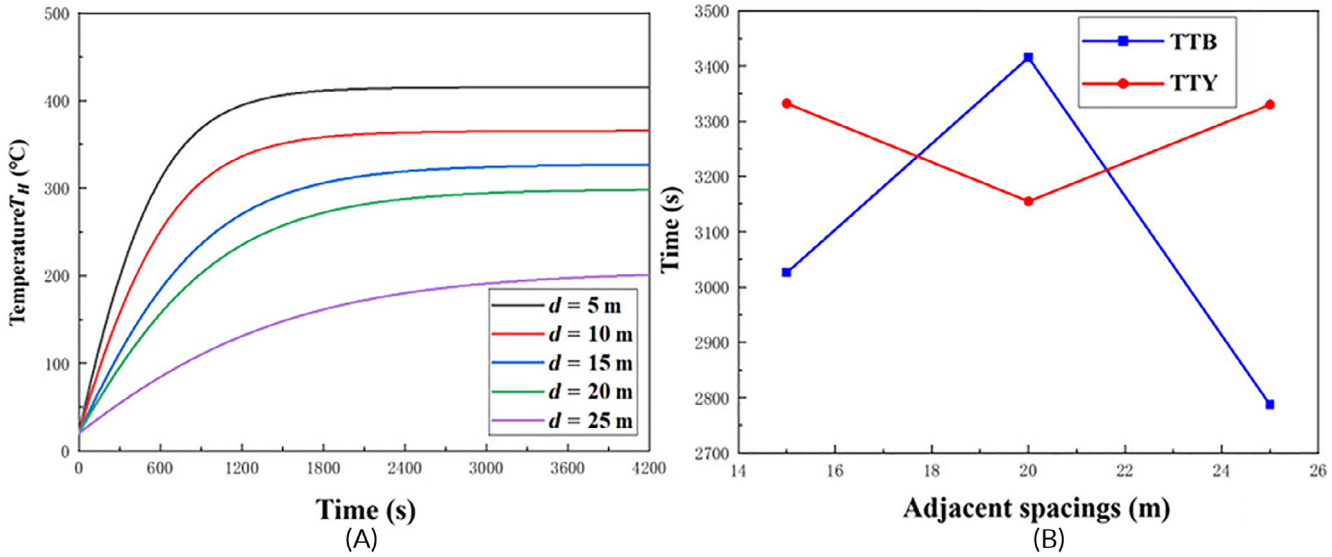

FIGURE 13 Parameter in thermal post-buckling and post-yielding under different adjacent spacings. (A) Comparison of T_H. (B) Comparison of time to buckling (TTB) and time to yielding (TTY).

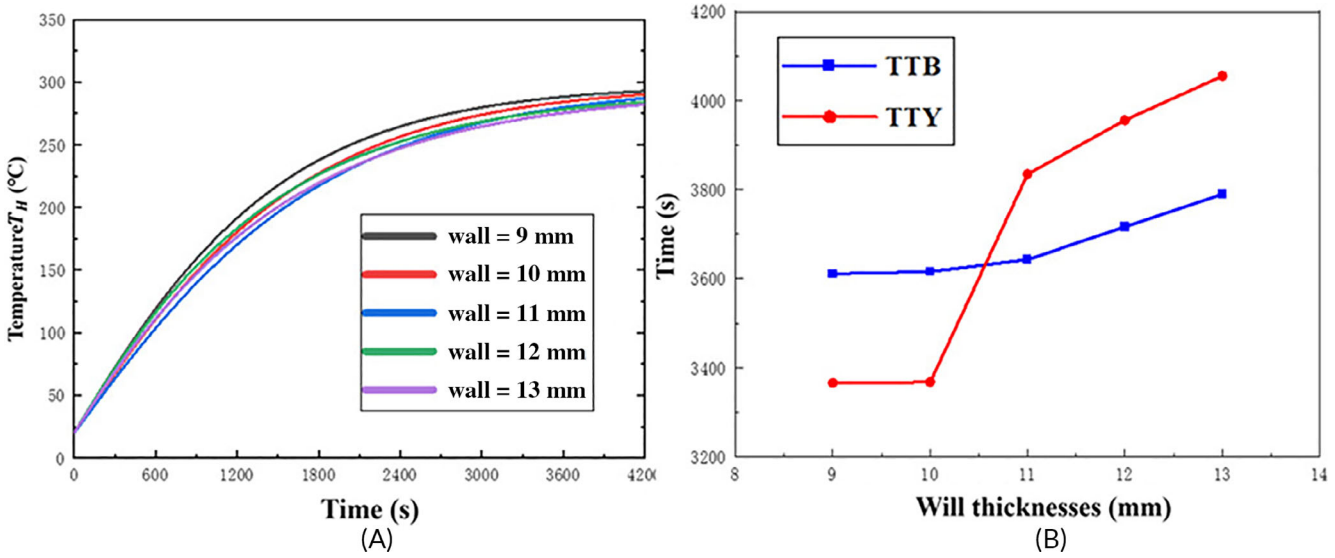

FIGURE 14 Parameter in thermal post-buckling and post-yielding in different wall thicknesses. (A) Comparison of T_H. (B) Comparison of time to buckling (TTB) and time to yielding (TTY).

illustrated in Figure 13A. It shows that T_H exhibits a negative correlation with the adjacent spacing. This phenomenon can be attributed to the thermal radiation to adjacent tank decreasing with the increase of the distance between the adjacent tank and the combustion tank, leading to the increase of heat loss in the heat transfer process. Figure 13B displays the comparative analysis of the TTB and TTY for the adjacent tank under different adjacent spacings. Table 3 summarizes the relevant parameters of adjacent tanks for various adjacent spacings (d). When $d \geq 20$ m, there is a negative correlation between the T_0 of the adjacent tank and the adjacent spacing, while the T_0 of the adjacent tank is positively correlated with adjacent spacing.

Both buckling and yielding do not occur under the adjacent spacings of 5, 10, and 30 m. This is because when the spacing is too small, the lower region of the tank receives a small amount of thermal radiation, and the temperature difference of the tank is weakened, which reduces the difference of thermal expansion. Therefore, the adjacent tank does not fail after heating, and only linear thermal expansion occurs. The TTB of the adjacent tank is extended as the adjacent spacing increases. However, when the adjacent spacing becomes excessively large ($d = 25$, 30 m), the TTB of the tank decreases or does not occur. This is attributed to a decrease in the heating rate of adjacent tanks, resulting in a decrease in temperature variability in different areas of the storage tank. The results can evaluate the reasonableness and safety of storage tank layout under fire safety engineering conditions.

4.4 | Effect of wall thicknesses

Section 4.1 investigated the influence of uniform and stepwise tanks. To explore the influence of wall thickness on failure modes and TTF and avoid noise caused by stepwise tanks, this section exclusively investigates the effects of the adjacent tank with different uniform wall thicknesses. Figure 14A illustrates the distribution in the maximum temperature (T_H) of the adjacent tank under different wall thicknesses. T_H is inversely correlated with the wall thickness of the storage tank. This can be attributed to the fact that when the thermal radiation energy from the combustion tank is constant, the heat resistance of the storage tank increases as the thickness of the adjacent tank increases, resulting in a smaller temperature difference between the inner and outer layers of the adjacent tank when the temperature rapidly changes. Figure 14B presents a comparison of the TTB and TTY of the adjacent tank under different wall thicknesses. Table 4 summarizes the relevant parameters of adjacent tanks for wall thickness (d_t). T_0 of the adjacent tank is inversely related to the tank's wall thickness. T_0 of the tank rises and the TTB and TTY extend as the wall thickness increases.

TABLE 4 Parameters corresponding to different wall thicknesses.

d_t (mm)	TTB (s)	T_0 (°C)	TTY (s)	T_S (°C)
9	3611	288.447	3366	272.015
10	3616	284.482	3368	274.086
11	3643	280.438	3835	274.606
12	3717	279.655	3956	274.630
13	3790	277.936	4055	276.024

Abbreviations: TTB, time to buckling; TTY, time to yielding.

When $d_t \leq 10$ mm, the failure mode of the adjacent tank is yielding. However, when $d_t > 10$ mm, the failure mode of the adjacent tank is buckling. This is because when the wall thickness is too small, it diminishes the tank's yield strength, decreases its resistance to deformation, and enhances its susceptibility to geometric deformation, ultimately resulting in a preference for yielding failure. On the other hand, as the wall thickness of the storage tank increases, it leads to

TABLE 5 Structural parameters of the storage tanks.

ID	Volume (m^3)	Diameter (m)	Height of wall (m)	Thickness of shell (mm)	Curvature radius of dome roof (m)	Thickness of roof (mm)
1	3000	15	17.8	6–10	18	6
2	5000	20	17.8	6–13	24	6
3	10,000	27.5	17.8	6–13	33	6

TABLE 6 Parameters corresponding to different volumes.

V (m^3)	T_H (°C)	TTB (s)	T_0 (°C)	TTY (s)	T_S (°C)
3000	301.427	3382	299.156	3233	298.422
5000	298.701	3711	297.834	3839	298.142
10,000	297.976	-	-	3988	297.588

uneven heating of the adjacent tank due to thermal radiation from the combustion tank. This elevates the heating rate which induces different degrees of structural deformation due to thermal expansion across different regions of the adjacent tank, causing nonlinear and significant deformations that contribute to the structural instability of the storage tank, resulting in a preferential buckling failure. The results can be applied to the safety evaluation of storage tank process structure in fire scenarios.

4.5 | Effect of volumes

To explore the role of tank volumes, the volumes of the adjacent tank are adjusted to 3000, 5000, and 10,000 m^3. The structural parameters for each volume are specified in Table 5, and the relevant parameters are summarized in Table 6. It can be observed that the maximum temperature (T_H) of the tank is inversely correlated with the tank's volume, and T_H of the adjacent tanks are relatively close to each other, with only a difference of 2–3°C. This similarity in temperatures can be attributed to the structural similarities among the tanks, which result in similar thermal radiation capacities. When the thermal radiation energy of the combustion tank is fixed, the temperature rise results of the adjacent tanks will be consistent.

When the tank volume is 10,000 m^3, the adjacent tank experiences yielding failure but not buckling failure. This is because when the volume is too large, the overall temperature difference of the storage tank is reduced, which reduces the difference of circumferential thermal expansion. Conversely, when the tank volume is 3000 m^3, yielding failure takes priority. This is because the temperature rise of the adjacent tank is the highest, resulting in the maximum temperature and the increase of the thermal stress of the adjacent tank. However, the wall thickness of the storage tank of 3000 m^3 tends to be the same, and the ratio of height to diameter is the largest, so the adjacent tank structure is more stable and the yield failure preferentially occurs.

When the tank volume is 5000 m^3, buckling failure becomes the priority. This phenomenon arises from several factors. Firstly, the diameter and the flame height of combustion tank of the adjacent tank are same as the combustion tank. This synchronicity amplifies the disparity of stepwise wall thickness at various points along the tank, leading to compromised structural stability. Consequently, it results in heightened temperature variability across different regions of the tank, intensifying thermal expansion. The nonuniform rate of thermal expansion among these diverse areas further exacerbates the risk of buckling. The results can be utilized to the determination of failure modes caused by different storage tank volumes in fire safety engineering.

5 | CONCLUSIONS

This study presented a comprehensive numerical simulation analyzing the thermal response of storage tanks exposed to fire scenarios. The primary objective was to investigate the failure modes of storage tanks，specifically focusing on buckling and yielding. The analysis took into account various factors such as the structural design of storage tanks (uniform or stepwise), the flame heights of combustion tank, adjacent spacings, wall thicknesses, and tank volumes.

The following summarizes the key findings:

- Failure modes: The predominant failure modes observed under thermal radiation are thermal buckling and yielding. The types of failure and the corresponding time to failure (TTB and TTY) exhibit variability based on tank structures, the flame heights of combustion tank, wall thicknesses, and other factors.
- Influence of flame heights of the combustion tank: Tanks experience buckling as the dominant failure mode when the flame height of combustion tank is below 20 m. Conversely, no failure occurs if the flame heights of combustion tank exceeds 20 m.
- Tank structure impact: Stepwise tanks tend to exhibit yielding as the primary failure mode, while uniform tanks are more prone to buckling under similar conditions.
- Wall thickness effect: Tanks with a wall thickness less than 10 mm predominantly fail due to yielding, whereas those with a thickness exceeding 10 mm are more susceptible to buckling.
- Tank volume influence: The failure mode is yielding for a tank volume of 3000 m^3, buckling for 5000 m^3, and yielding again for 10,000 m^3.

These findings offer valuable insights into predicting failure modes and TTF in storage tanks during fire incidents. The results can

significantly contribute to informed decision making in emergency response situations, particularly regarding fire-induced domino effects.

Looking ahead, future research may involve the development of simulation-based failure models to rapidly predict tank failures. This could include the consideration of additional factors such as materials to enhance prediction accuracy. The ultimate goal is to continually improve our understanding of storage tank behavior in fire accidents and refine emergency response strategies accordingly.

AUTHOR CONTRIBUTIONS

Li Mo: Methodology; resources; supervision; writing – original draft; writing – review and editing. **Shenbin Xiao:** Validation; writing – original draft. **Hang Chen:** Resources; software. **Xinxin Tan:** Data curation; formal analysis; software; writing – original draft. **Ming Yang:** Supervision; writing – review and editing. **Genserik Reniers:** Methodology; supervision. **Chao Chen:** Conceptualization; methodology; resources; supervision; writing – review and editing.

FUNDING INFORMATION

This study was supported by Science and Technology Department of Sichuan Province (Sichuan Province Science and Technology Support Program 2023YFS0412).

CONFLICT OF INTEREST STATEMENT

The authors declare no conflicts of interest.

DATA AVAILABILITY STATEMENT

None.

ORCID

Genserik Reniers https://orcid.org/0000-0001-9592-1811
Chao Chen https://orcid.org/0000-0002-1443-8017

REFERENCES

1. Tan X, Xiao S, Yang Y, Khakzad N, Reniers G, Chen C. An agent-based resilience model of oil tank farms exposed to earthquakes. Alma Mater Studiorum – Università di Bologna, Dipartimento di Ingegneria Civile, Chimica, Ambientale e dei Materiali (DICAM), LISES, via Terracini no 28, 40131 Bologna, Italy Safety and Security Science Group, Fa. 2024;247:110096. doi:10.1016/j.ress.2024.110096
2. Jing W, Wang J, Cheng X. Dynamic responses of oil storage tank considering wind interference effect. *Eng Fail Anal*. 2019;104:1053-1063. doi:10.1016/j.engfailanal.2019.06.040
3. Khakzad N, Reniers G. Risk-based design of process plants with regard to domino effects and land use planning. *J Hazard Mater*. 2015;299:289-297. doi:10.1016/j.jhazmat.2015.06.020
4. Khan FI, Abbasi SA. Estimation of probabilities and likely consequences of a chain of accidents (domino effect) in Manali Industrial Complex. *J Clean Prod*. 2001;9(6):493-508. doi:10.1016/s0959-6526(01)00008-7
5. Khan FI, Abbasi SA. An assessment of the likelihood of occurrence, and the damage potential of domino effect (chain of accidents) in a typical cluster of industries. *J Loss Prev Process Ind*. 2001;14(4):283-306. doi:10.1016/s0950-4230(00)00048-6
6. Reniers G, Faes R. 13 – Managing domino effects in a chemical industrial area. In: Reniers G, Cozzani V, eds. *Domino Effects in the Process Industries*. Elsevier; 2013:272-295. doi:10.1016/b978-0-444-54323-3.00013-0
7. Jaca RC, Godoy LA, Calabró HD, Espinosa SN. Thermal post-buckling behavior of oil storage tanks under a nearby fire. *Int J Press Vessel Pip*. 2021;189:104289. doi:10.1016/j.ijpvp.2020.104289
8. Chen C, Reniers G, Zhang L. An innovative methodology for quickly modeling the spatial-temporal evolution of domino accidents triggered by fire. *J Loss Prev Process Ind*. 2018;54:312-324. doi:10.1016/j.jlp.2018.04.012
9. Ding L, Ji J, Khan FI. Combining uncertainty reasoning and deterministic modeling for risk analysis of fire-induced domino effects. *Saf Sci*. 2020;129:104802. doi:10.1016/j.ssci.2020.104802
10. Zhang L, Landucci G, Reniers G, Khakzad N, Zhou J. DAMS: a model to assess domino effects by using agent-based modeling and simulation. *Risk Anal*. 2018;38(8):1585-1600. doi:10.1111/risa.12955
11. An Han H, Han I, McCurdy S, et al. The intercontinental terminals chemical fire study: a rapid response to an industrial disaster to address resident concerns in Deer Park, Texas. *Int J Environ Res Public Health*. 2020;17(3):986. doi:10.3390/ijerph17030986
12. Wu Z, Hou L, Wu S, Wu X, Liu F. The time-to-failure assessment of large crude oil storage tank exposed to pool fire. *Fire Saf J*. 2020;117:1. doi:10.1016/j.firesaf.2020.103192
13. Salahshour S, Fallah F. Elastic collapse of thin long cylindrical shells under external pressure. *Thin-Walled Struct*. 2018;124:81-87. doi:10.1016/j.tws.2017.11.058
14. Yang JH, Zhang MG, Zuo YW, Cui XM, Liang CQ. Improved models of failure time for atmospheric tanks under the coupling effect of multiple pool fires. *J Loss Prev Process Ind*. 2023;81. doi:10.1016/j.jlp.2022.104957
15. Liu H, Jiang J, Li Y, Ni L, Wang J. Coupling effects of the explosion shock wave and heat radiation on the dynamic response of a fixed-roof tank. *J Loss Prev Process Ind*. 2021;72:104534. doi:10.1016/j.jlp.2021.104534
16. Birk AM, Yoon KT. High-temperature stress-rupture data for the analysis of dangerous goods tank-cars exposed to fire. *J Loss Prev Process Ind*. 2006;19(5):442-451. doi:10.1016/j.jlp.2005.11.003
17. Rebec A, Plešec P, Kolšek J. Pool fire accident in an aboveground LFO tank storage: thermal analysis. *Fire Saf J*. 2014;67:135-150. doi:10.1016/j.firesaf.2014.05.022
18. Wang X, Zhou K, Mébarki A, Jiang J. Numerical simulation of thermal response behavior of floating-roof tanks exposed to pool fire. *Appl Therm Eng*. 2020;179:115692. doi:10.1016/j.applthermaleng.2020.115692
19. Batista-Abreu JC, Godoy LA. Thermal buckling behavior of open cylindrical oil storage tanks under fire. *J Perform Constr Facil*. 2013;27(1):89-97. doi:10.1061/(asce)cf.1943-5509.0000309
20. Landucci G, Gubinelli G, Antonioni G, Cozzani V. The assessment of the damage probability of storage tanks in domino events triggered by fire. *Accid Anal Prev*. 2009;41(6):1206-1215. doi:10.1016/j.aap.2008.05.006
21. Liu Y. *Thermal Buckling of Metal Oil Tanks Subject to an Adjacent Fire*. University of Edinburgh; 2015.
22. Godoy LA, Batista-Abreu JC. Buckling of fixed-roof aboveground oil storage tanks under heat induced by an external fire. *Thin-Walled Struct*. 2012;52:90-101. doi:10.1016/j.tws.2011.12.005
23. Cozzani V, Reniers G. Special issue: domino effects in the process industry – advancing the state of the art. *Reliab Eng Syst Saf*. 2015;143:1-2. doi:10.1016/j.ress.2015.08.001
24. Pantousa D. Numerical study on thermal buckling of empty thin-walled steel tanks under multiple pool-fire scenarios. *Thin-Walled Struct*. 2018;131:577-594. doi:10.1016/j.tws.2018.07.025
25. Li Y, Jiang J, Zhang Q, et al. Static and dynamic flame model effects on thermal buckling: fixed-roof tanks adjacent to an ethanol pool-fire. *Process Saf Environ Prot*. 2019;127:23-35. doi:10.1016/j.psep.2019.05.001
26. Dong X, Ding X, Li G, Lewis GP. Stiffener layout optimization of plate and shell structures for buckling problem by adaptive growth method.

Struct Multidisc Optim. 2020;61(1):301-318. doi:10.1007/s00158-019-02361-0
27. Pantousa D, Godoy LA. On the mechanics of thermal buckling of oil storage tanks. *Thin-Walled Struct*. 2019;145:106432. doi:10.1016/j.tws.2019.106432
28. Pourkeramat A, Daneshmehr A, Jalili S, Aminfar K. Investigation of wind and smoke concentration effects on thermal instability of cylindrical tanks with fixed roof subjected to an adjacent fire. *Thin-Walled Struct*. 2021;160:107384. doi:10.1016/j.tws.2020.107384
29. Li Y, Jiang J, Yu Y, Wang Z, Xing Z, Zhang Q. Thermal buckling of oil-filled fixed-roof tanks subjected to heat radiation by a burning tank. *Eng Fail Anal*. 2022;138(suppl C):106393. doi:10.1016/j.engfailanal.2022.106393
30. Li Y, Jiang J, Yu Y, Wang Z, Xing Z, Zhang Q. Fire resistance of a vertical oil tank exposed to pool-fire heat radiation after high-velocity projectile impact. *Process Saf Environ Prot*. 2021;156(suppl C):231-243. doi:10.1016/j.psep.2021.10.013
31. *Welded Steel Tanks for Oil Storage*. 10th ed. Addendum 1, January 2000; Addendum 2, November 2001; Addendum 3, September 2003:280.
32. Chen C, Chen H, Mo L, et al. Buckling failure analysis of storage tanks under the synergistic effects of fire and wind loads. Faculty of Engineering and Applied Sciences, The Memorial University of Newfoundland, St John's, Newfoundland A1B 3X5, Canada; Centre for Pollution Control and Energy Technology, Pondicherry Universi. 2024;87:105208. doi:10.1016/j.jlp.2023.105208
33. Mudan KS. Thermal radiation hazards from hydrocarbon pool fires. *Prog Energy Combust Sci*. 1984;10(1):59-80. doi:10.1016/0360-1285(84)90119-9
34. Zhou K, Wang X. Thermal radiation modelling of pool fire with consideration on the nonuniform temperature in flame volume. *Int J Therm Sci*. 2019;138:12-23. doi:10.1016/j.ijthermalsci.2018.12.033
35. Rew PJ, Hulbert WG. *Development of Pool Fire Thermal Radiation Model*. HSE Contract Research Report; 1996.
36. Mansour KA. *Fires in Large Atmospheric Storage Tanks and Their Effect on Adjacent Tanks*. Loughborough University; 2012.
37. Johnson A, Brightwell H, Carsley A. A model for predicting the thermal-radiation hazards from large-scale horizontally released natural-gas JET fires. *Trans IChemE*. 1994;72(B3):157-166.
38. Thomas PH. The size of flames from natural fires. Ninth Symposium (International) on Combustion. 1963:844-859. doi:10.1016/b978-1-4832-2759-7.50093-5
39. Hurley MJ, Gottuk D, Hall JR, Harada K, Kuligowski E, Puchovsky M, Torero J, Watts JM, Wieczorek C, eds. *SFPE Handbook of Fire Protection Engineering*. New York: NY Springer; 2008. 1700 p.
40. Espinosa SN, Jaca RC, Godoy LA. Thermal effects of fire on a nearby fuel storage tank. *J Loss Prev Process Ind*. 2019;62:103990. doi:10.1016/j.jlp.2019.103990
41. Beyler CL. Fire hazard calculations for large, open hydrocarbon fires. In *SFPE Handbook of Fire Protection Engineering*. Morgan J, Hurley PE, Daniel GPE,John RH (eds). Springer; 2016:2591-2663. doi:10.1007/978-1-4939-2565-0_66
42. Santos F, Landesmann A. Thermal performance-based analysis of minimum safe distances between fuel storage tanks exposed to fire. *Fire Saf J*. 2014;69:57-68. doi:10.1016/j.firesaf.2014.08.010

How to cite this article: Mo L, Xiao S, Chen H, et al. Numerical study of failure modes of hazardous material tanks exposed to fire accidents in the process industry. *Process Saf Prog*. 2024; 1-14. doi:10.1002/prs.12643